A Low-Profile Supercapacitor-Based Normal and Shear Force Sensor

Ye Zhang, A. Serdar Sezen, and Rajesh Rajamani, *Senior Member, IEEE*

***Abstract*—This paper focuses on the development of a thin normal-shear force sensor based on the use of a supercapacitive sensing mechanism. The sensor has a quad structure with four sensing units in which the bottom substrate has four pairs of electrodes while the top deformable portion has a solid-state electrolyte. The application of normal and shear forces increases the contact area between the solid-state electrolyte and the electrodes. Key innovations in the sensing mechanism include the use of a paper-based solid state electrolyte, the use of 3d-printing with a combination of soft and hard polymers to construct the top portion of the sensor, and the use of deep learning to model the sensor response. The sensor can accept any combination of shear and normal forces and can measure both their magnitudes and orientation. The deep learning based sensor response model enables accurate sensor calibration while accommodating the imperfections in the stiffness distribution of the sensor. The normal and shear force sensitivities are of the order of 50 nF/N and 22 nF/N respectively, which are orders of magnitude larger than the sensitivity of a traditional capacitive force sensor.**

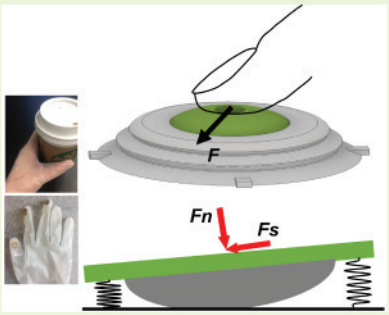

***Index Terms*—Force sensors, sensor calibration, shear and normal force sensors, supercapacitive sensor, deep learning.**

I. Introduction

SENSORS for measurement of normal forces are inexpensive and easily available. One example of an easily available thin film normal force sensor is the Tekscan sensor [1]. However, in many applications, it is necessary to measure both the normal and shear forces at the sensor location. For example, consider a wearable device like an instrumented glove that is used to measure the forces applied by an operator in a skilled task [2] as shown in Fig. 1. Such gloves can be used on surgeons to learn about the surgical manipulations they perform [3], by sportsmen to learn and improve on the actions performed in sports [4], in healthcare to help a prosthetic hand with controls or rehabilitation [5], [6], and in laboratories to learn about grasping and other hand manipulations of human subjects [7], [8]. Current sensors that can measure both normal and shear forces can be bulky and highly expensive. For example, the ATI 6-axis force sensor has a price over $6000 and has a size exceeding $1 \times 1 \times 1\ in^3$, so that it cannot really be used for an instrumented glove or other low-profile applications. This paper focuses on the development of a thin sensor that can measure both normal and shear forces. The developed sensor has a very high force sensitivity due to its use of a supercapacitive sensing mechanism. This paper describes the challenges in developing such a sensor, describes the design and fabrication of the sensor, and documents its experimental performance.

Previously in literature, several different groups have been developing shear and/or normal force sensors based on different sensing principles for measuring forces on the fingertips. Piezoresistive and piezoelectric force sensors have been widely explored due to their ease of micro-fabrication [9]–[13]. Piezoresistive sensors, however, suffer from problems like hysteresis, drift, creep and temperature dependency [11], [14]. Optical sensors have also been applied for measuring shear forces combining a trapezoidal external metallic frame with an integrated micro optical displacement sensor [15], [16]. However, these sensors measure only shear force and lack the capability of measuring normal force. Besides, these sensors cannot meet the requirements of being soft and compact for wearable applications. Due to low temperature and pressure hysteresis, low power consumption and ease of fabrication,

Manuscript received June 3, 2020; accepted July 15, 2020. Date of publication August 4, 2020; date of current version December 4, 2020. This work was supported in part by the National Science Foundation under Grant EFMA 1830958. The associate editor coordinating the review of this article and approving it for publication was Dr. Emiliano Schena. *(Corresponding author: Rajesh Rajamani.)*

Ye Zhang and Rajesh Rajamani are with the Department of Mechanical Engineering, The University of Minnesota at Twin Cities, Minneapolis, MN 55455 USA (e-mail: zhan3068@umn.edu; rajamani@umn.edu).

A. Serdar Sezen is with the Department of Mechanical Engineering, St. Cloud State University, St. Cloud, MN 56301 USA (e-mail: ssezen@stcloudstate.edu).

Digital Object Identifier 10.1109/JSEN.2020.3014174

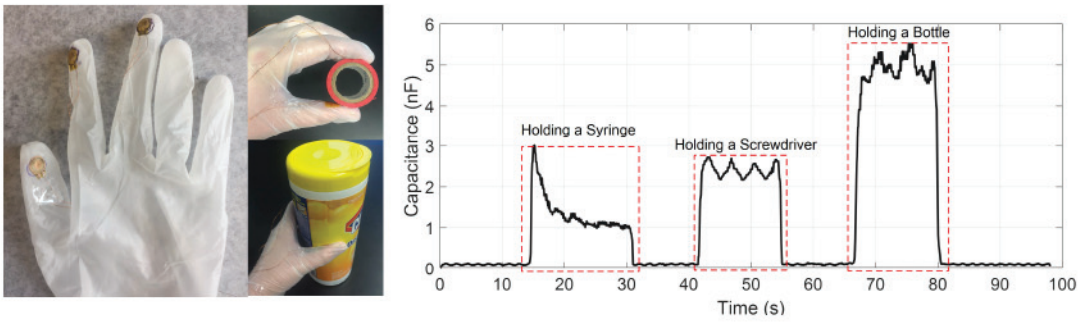

Fig. 1. Measuring shear and normal forces while handling various objects wearing an instrumented glove.

capacitive pressure sensing has been highly explored for use in tactile sensors [17]–[28]. However, capacitive sensors have limitations of trade-off between sensing range and sensitivity, and have significant susceptibility to parasitic noise [29].

In terms of sensor design, most of the sensors above cannot provide measurements of shear force from arbitrary directions due to their directional structural design. Charalambides and Bergbreiter [30] and Viry *et al.* [18] developed 3-axis capacitive shear and normal force sensors which used a square shape design, and the sensors' performance was only investigated in two major directions of the sensor. Shi, *et al.* developed an EGaln-based flexible piezoresistive shear and normal force sensor making use of a circular design which can measure force omni-directionally [14]. However, no experimental data was obtained under a combination of both normal and shear force. None of the shear and normal force sensors developed by other researchers have extensive experimental data taken from arbitrary directions to validate the performance of the sensors. A force sensor that can measure omnidirectional shear forces is valuable for real applications. Since in most cases, shear and normal forces exist simultaneously and they are deeply coupled, it is difficult to build a 3D analytical model for a sensor that is able to estimate normal and shear forces at the same time. Some researchers used finite element parametric studies [30], [31] to investigate the relation between material deformation and measured outputs (capacitance change, voltage change, etc.), however, the outputs are not directly related to force changes. For a 1D or 2D load, experimental calibration and curve fitting method could be used to estimate forces. For a 3D problem, however, due to the complexity of coupling of normal and shear forces, experimental calibration at every combination of normal and shear force is not feasible.

The specific unique contributions of this paper compared to others in literature include the following:

i) The developed shear and normal force sensor has an omni-directional structure capable of multi-axis sensing.
ii) A rapid and simple fabrication process that utilizes micro-fabrication only for the electrodes and utilizes 3d-printing for the rest of the structure reduces fabrication time and costs.
iii) A new supercapacitive sensing mechanism is exploited for measuring normal and shear forces simultaneously, providing ultra-high sensitivity (1000 times more sensitive than traditional capacitive sensors). Other supercapacitive sensors in literature have only been designed to measure normal forces [34].
iv) A deep-learning algorithm is used to develop a sensor response model based on a neural network that can provide accurate estimates of shear and normal forces. This sensor model enables the system to provide accurate shear and normal force readings irrespective of the force direction and irrespective of the variations in sensor stiffness around the circumference of the device that exist due to manufacturing imperfections.

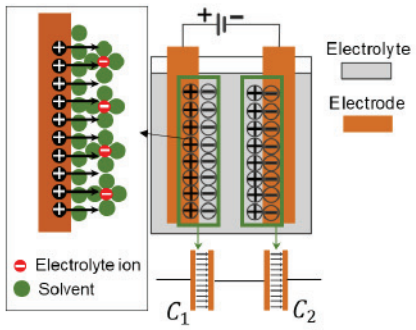

Fig. 2. Schematic of a supercapacitor: two electrodes in an electrolyte solution.

The outline of the rest of this paper is as follows. In section II, the design and fabrication details of the normal-shear force sensor are presented. In section III, various experimental methods are used to evaluate the performance of the sensor and to generate data for training a deep neural network model to represent the sensor response. Experimental results are presented in Section IV along with discussion of the results. Conclusions are presented in section V.

II. Sensor Design and Fabrication

Supercapacitive sensors, are also known as iontronic sensors.

A. Supercapacitive Sensing

Supercapacitors, also known as ultracapacitors, have been widely used previously for energy storage, but their use for sensing is a relatively new research area. A supercapacitor typically consists of two electrodes and a liquid electrolyte, as shown in Fig. 2. At each electrode-electrolyte interface, the positive and negative charges are separated from each other by a very small distance resulting in a 'double-layer' capacitor.

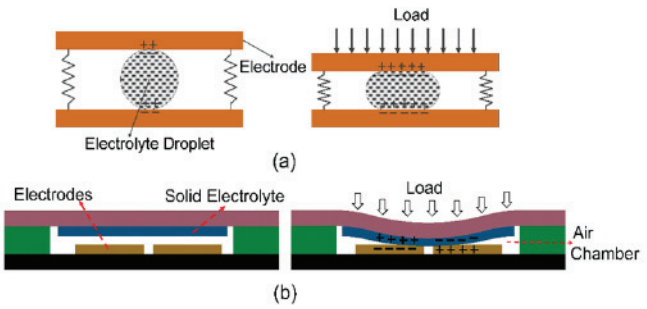

Fig. 3. Sensing mechanism of a supercapacitive sensor with (a) liquid electrolyte; (b) solid electrolyte.

A supercapacitor is governed by the same fundamental equation (1) as a traditional capacitor in which capacitance (c) can be described by

$$C = \frac{\varepsilon A}{d} \tag{1}$$

where A is the geometric surface area of the electrodes; ε is the relative permittivity of the dielectric material; and d is the distance between two oppositely biased electrodes. However, the distance d is extremely small (on the order of the distance between ions at an electrode-electrolyte layer, or just a few angstroms). Due to this small distance, a supercapacitor has very high capacitances, often measured in nF/cm^2 or even $\mu F/cm^2$.

In the use of a supercapacitor as a force sensor, a change in force is translated into a change in contact area between the electrodes and the electrolyte, and consequently results in a change in capacitance. Previous research on supercapacitive force sensors typically employed liquid-state electrolytes [32], [33]. An example of such a sensor is shown in Fig. 3 (a) with an electrolyte droplet being confined between two parallel electrodes [33]. This sensor provides high sensitivity and resolution. However, developing a miniaturized version of this sensor requires addressing some challenges. In order to avoid the complexity of using liquid electrolyte, a solid-state electrolyte is preferable to replace a liquid-state electrolyte. The deformation of a solid electrolytes in response to an applied force and the resulting change in its contact area with the electrodes can then be used to sense the applied force (Fig. 3 (b)).

A novel paper-based solid electrolyte was recently developed in our group [34] and used for supercapacitive sensors. This solid-state electrolyte is made by introducing active materials into the porous matrix of paper and functionalizing the entire thickness of the paper. This paper-based solid electrolyte provides enhanced mechanical elasticity properties, which enables the fabrication of supercapacitive sensors of high sensitivity. Further, using paper as a substrate provides easy configurability for fabricating the sensor. The schematic of a supercapacitive sensor using the paper-based solid electrolyte is shown in Fig.3 (b). The flexible electrolyte is deformed as load is applied and makes contact with the bottom electrodes, consequently creating a capacitance change. In a supercapacitor, due to the thin dielectric layer and high surface area electrodes, the capacitance of a supercapacitor is at least 3 orders of magnitude higher than the parasitic capacitance in a traditional capacitor, which makes the parasitic capacitance negligible [29]. In this paper, the shear and normal force sensor is developed as an interesting real-world application of the paper-based solid electrolyte.

B. Sensor Design

This section proposes a sensor design to simultaneously measure normal and shear forces using the supercapacitive sensing mechanism. The design schematic is shown in Fig. 4 including a top part (sideview) containing the solid electrolyte and a bottom substrate (top view) with all the electrodes. Each force sensing cell consists of 4 internal individual force units (S_1, S_2, S_3, S_4), that are axisymmetrically distributed. Each of the 4 force units has two electrodes. The electrodes are patterned in a circle in such a way that the four sensors lie symmetrically on the axes of a Cartesian coordinate system with the center of the eight electrodes sitting at the origin. The upper electrolyte is cured on the surface of a soft semi-ellipsoid. This soft semi-ellipsoid is assembled over the electrodes. If only normal force is applied as shown in Fig. 4 (b), the contact area between the electrodes and electrolyte increases, resulting in an increase in capacitance of all the four sensing units. If a combination of normal and shear forces is applied (Fig. 4 (c)), the center of the contact area shifts accordingly depending on the direction of the shear force, with the readings from the four force sensing units being different. Unlike Fig. 3, here the electrolyte is designed to be initially in contact with the electrode (even for zero force) in order to remove any dead zone in the sensor readings.

A more detailed physical structure of the proposed sensor design is shown in Fig. 5. The 4 pairs of electrodes in the bottom are patterned in a circle on a soft substrate. The top part contains a chamber made of both soft and hard material. It consists of a hard cap, a hard mesh, a soft semi-ellipsoid substrate to host the solid electrolyte and a soft side wall. The hard cap (Fig. 5(a)) is designed for better receiving the force applied from the top. A hard mesh (or skeleton) is printed and embedded inside the soft side wall to increase the elasticity and quick spring-back of the sensor (Fig. 5(c) and (d)). The solid electrolyte is cured on the surface of the soft semi-ellipsoid, which can deform under the applied force. The 4 capacitance readings (C_1, C_2, C_3, C_4) of the 4 sensors are used to estimate the normal force and shear force applied on the sensing cell.

C. Sensor Fabrication

The sensor was fabricated using MEMS fabrication techniques and 3D printing. The top part is made using multi-material 3D printing technology, combining materials of different flexibility properties in a single part. The bottom electrodes are patterned on a soft substrate through a sequence of MEMS fabrication processes.

1) Fabrication of the Bottom Electrodes: The bottom electrodes are fabricated on a flexible substrate, namely a polyimide (PI) film (Pyralux Copper Kapton Laminate, Dupont), using MEMS fabrication technologies, as shown in Fig. 6 (a).

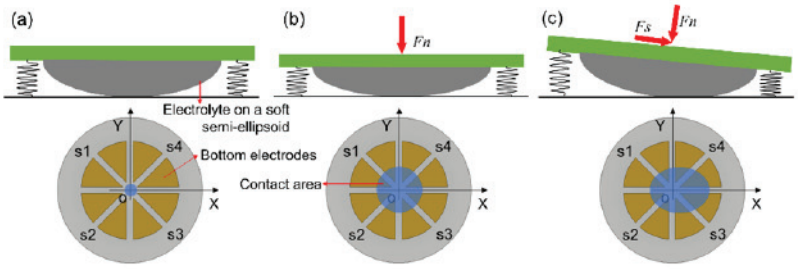

Fig. 4. Working mechanism of the supercapacitive normal and shear sensor (a) no force is applied, (b) normal force is applied, (c) both normal and shear force are applied.

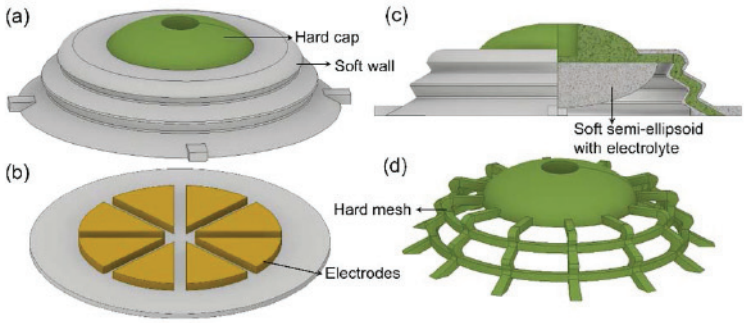

Fig. 5. Schematic of the normal and shear force sensor (a) top chamber with the solid electrolyte, (b) bottom electrodes patterned on a soft substrate, (c) three quarter section view of the top chamber, (d) a hard mesh embedded in the soft wall.

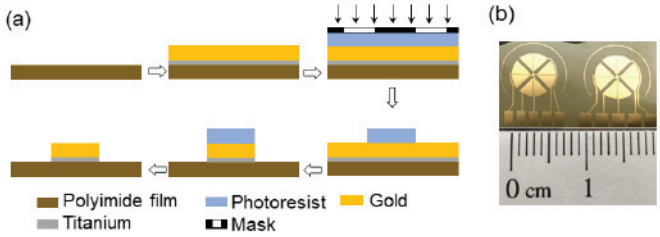

Fig. 6. (a) Fabrication process of the bottom electrode. (b) The electrodes patterned on PI substrate.

PI film is lightweight, flexible, resistant to heat and chemicals, and thus widely used as an electronic circuit substrate. The PI film is first cut into silicon-wafer size for the ease of fabrication in the following procedures, before solvent cleaning and deionized (DI) water rinsing to remove residuals. After nitrogen blow-dry, the film is transferred to a hot plate at $120°C$ $(1min)$. The electrode materials are sputtered onto the PI film from source target (AJA II-Sputter System). First, a thin layer of titanium (20nm) is sputtered on the polyimide film for enhancing adhesion before sputtering a gold layer (200nm). The top surface of gold is the effective electrode material for sensing. The electrolyte contacts the gold electrodes upon loading. A drop of water is put on a clean silicon wafer before transferring the PI film onto it with the gold side facing up. This combination is then loaded to a spinner that is then ran for 30s at 3000rpm. By doing this, the soft PI film can stick very well to the bottom silicon wafer, due to the existence of the evenly spread water layer between the soft film and silicon wafer. This process makes it easier to handle the film in the following alignment process, and can be repeated if necessary due to the evaporation of water layer and bubble generation. Then, the 8 electrodes are patterned in a circle (6mm in diameter) using photolithography and wet etching. A transparency printed photomask is used for photolithography (25400 dpi, CAD/Art Services, Inc.), which offers a cheaper and flexible option compared to a chrome-based mask. A positive photoresist, AZ 1505, is coated on the gold surface for 30s at 3000 rpm. After soft-baking at 80°C for 60s, it is exposed for 2.5s $(12mW/cm^2)$ followed by 60s post-exposure bake at 90°C. It is then developed in 351 solution (developer: DI water = 1:5) for 30s and rinsed in DI water for 2 mins and blow-dried. Then it is dipped to gold etchant solution (GE-8148, Transene) for about 30s and transferred to the Titanium etchant (HF, Hydrogen Peroxide, Water 1:1:20) for about 15s. After cleaning, the as-fabricated electrode on PI substrate is shown in Fig. 6 (b).

2) Fabrication of the Flexible Sensor Top: The paper-based solid electrolyte is cured on the surface of an ellipsoid structure inside a 3D printed chamber as shown in Fig 7. 3D printing is an additive manufacturing technology in which material is fused under computer control to create a three-dimensional object, with material being added together, typically layer by layer [35]. 3D printing has experienced rapid technological advances in recent years, and is capable of printing feature size up to a few microns accuracy and seamlessly integrating materials with different physical properties into the same part. Here, the top chamber is made using multi-material 3D printing technology (Stratasys J750 PolyJet 3D Printer), combining materials of different properties in a single part. The structure contains a soft side wall, a soft ellipsoid, a hard cap, and a

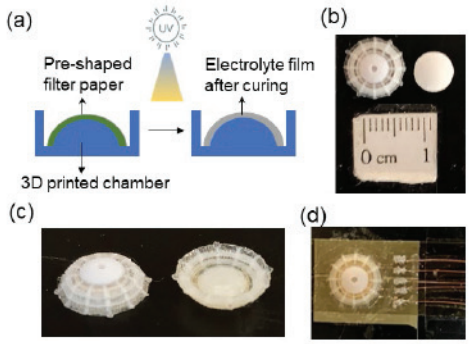

Fig. 7. (a) Fabrication of the electrolyte. (b) 3D printed chamber and the pre-shaped filter paper. (c) the solid electrolyte cured inside the soft chamber. (d) Photograph of the assembled normal and shear force sensor.

TABLE I
MATERIALS FOR THE SENSOR

Part Name	Product Name/Specification	Manufacturer/ Provider
3D printing soft materials	Agilus30/shore hardness 27 -35 Scale A	Stratasys
3D printing hard materials	Vero/ shore hardness 83 – 86 Scale D	Stratasys
Sealant	Clear Silicone Waterproof Sealant	Loctite
Substrate of the electrodes	Polyimide 75μm, 300 HPP-ST	Dupont
Connecting wires	40 AWG, enamel wires	Elektrisola
Filter paper	HATF, 0.45um	MF-Millipore
Ionic liquid	1-ethyl-3-methylimidazolium tricyanomethanide [EMIM][TCM]	IOLITEC Inc.
Prepolymer	PEG diacrylate (PEGDA, Mw = 575 g/mol) monomers	Sigma–Aldrich
Photo initiator	2-hydroxy-2-methylpropiophenone (HOMPP)	Sigma–Aldrich

hard mesh. The materials with different properties are specified in Table I. It should be noted that the elasticity of each part can be customized. The soft part provides deformation upon loading which consequently results in capacitance changes in the sensor. The hard cap is printed for the purpose of better receiving forces applied on top, while a hard mesh (or skeleton, white color in Fig. 7 (c)) is embedded inside the soft body and designed to improve the elasticity of the structure. The feature size of the mesh strands is around 300um.

3) Fabrication of Sensing Deformable Membrane With Electrolyte: The fabrication process for the solid electrolyte is shown in Fig. 7 (a), which starts from cutting the filter paper into a circular shape (Fig. 7 (b)). The circular filter paper is pre-shaped into a dome shape using two molds. The paper is placed between the two matching molds and then pressure is applied on this combination using clamps for more than 24 hours. After releasing the molds, a paper dome is obtained. The dome is then transferred to the top of the soft ellipsoid of the 3D printed chamber. An ionic liquid, a prepolymer solution, and a photo initiator are mixed in the ratio of 5:4:1 by weight by sonicating. The mixed gel is then brushed on to the filter paper, that functionalizes the entire thickness of the paper. After that, the combination was put under UV light (~325 nm, 36W) in a glovebox (inert environment filled with nitrogen) at room temperature for 1 min. A clear film (150um) sticking to the 3D printed chamber is obtained. It should be noted that the ratio of the components can be changed to achieve solid electrolytes with different mechanical properties. The materials details are listed in Table I. The details for making the solid electrolyte can be found in our previous research [34]. The 3D printed chamber with electrolyte is shown in Fig. 7 (c). This novel paper-based solid electrolyte has excellent mechanical properties as shown in Table II. It is highly flexible and stretchable. In comparison with the ionic-gel electrolyte without using paper, the ultimate tensile strength (maximum stress before failure) of the paper-based electrolyte is 50% larger, the toughness 3.55 times higher and the maximum elongation strain 2.5 times larger. The Young's modulus of the paper-based electrolyte is only about half of the Young's modulus of the ionic-gel electrolyte. The adding of cellulose fibers weakens the crystallinity of the gel and improves the softness and extensibility properties of the electrolyte film. Besides, the ease of making paper substrates of different shapes allows us to easily construct electrolytes of various complicated 3D geometries.

TABLE II
PROPERTIES OF THE PAPER-BASED SOLID ELECTROLYTE

Young's Modulus (MPa)	Ultimate tensile strength (MPa)	Toughness (N/m^2)	Configurability
4.6	3.06	20.1×10^6	Various geometries: arch, cylinder, spiral, etc.

4) Sensor Assembly: The soft chamber with the cured electrolytes was then assembled over the electrodes using sealing glue (Loctite, Waterproof Sealant). Connecting wires (40 AWG, enamel wires) are soldered onto the electrical contact pads on the PI substrate. The other ends of the wires are connected to 4 jumper wires for easy connection to the measurement equipment. The assembled sensor with 4 supercapacitive sensing units is shown in Fig. 7 (d). The assembled sensor is about 2mm in thickness. The desired overall size of the sensor was first determined to be 8mm in diameter, so as to be suitable for applications such as the instrumented glove. The area of contact on top of the sensor was approximately 0.5 cm. This was an ideal size in the sense that the area was not too large but was appropriate for the type of unit modular force measurement needed on a glove finger. At the same time, this area was adequate to enable measurement of normal and shear components (and direction of load) accurately.

D. Learning of the Sensor Response

The developed sensor is an omni-directional sensor in which forces can be applied on the sensor in any direction. While the sensor was designed to be axisymmetric, manufacturing imperfections during 3D printing make the stiffness and hence the

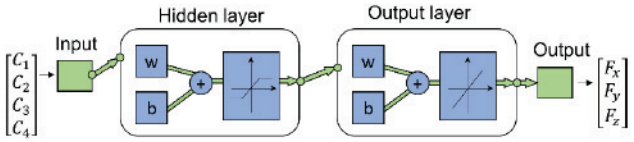

Fig. 8. Schematic of the neural network.

sensitivity of the sensor vary depending on the circumferential location in which the forces are applied.

In order to obtain a sensor response that is accurate and correctly provides the shear and normal components of the force, no matter in which direction forces are applied, a learning algorithm is developed for calibration of the sensor. In order to provide accurate estimates of the shear and normal forces acting on the top of the sensor, an accurate sensor model must be used to fully map from individual force unit readings to the total applied normal and shear forces. For a linear sensor with axisymmetric stiffness, the normal force can be obtained from the average of the four force units as

$$F_z = \frac{1}{4}(K_{n1}C_1 + K_{n2}C_2 + K_{n3}C_3 + K_{n4}C_4) \quad (2)$$

where K_{n1}, K_{n2}, K_{n3} and K_{n4} are the calibration coefficients between normal force and capacitance of each sensor.

The shear force along the x axis can be obtained from:

$$F_x = |(K_{s3}C_3 + K_{s4}C_4) - (K_{s1}C_1 + K_{s2}C_2)| \quad (3)$$

While the shear force along the y axis can be obtained from:

$$F_y = |(K_{s1}C_1 + K_{s4}C_4) - (K_{s3}C_3 + K_{s2}C_2)| \quad (4)$$

where K_{s1}, K_{s2}, K_{s3} and K_{s4} are the calibration coefficients between shear force and capacitance of each sensor.

However, the shear and normal force sensor response of the fabricated device does not follow the ideal equations (2), (3) and (4). Instead the sensor response is non-linear and varies with circumferential location due to significant manufacturing imperfections from 3d-printing. That can make accurately building an analytical sensor model very difficult in practice. Therefore, a generalized regression neural network [36]–[38] was used in order to obtain a model and matching the experimental data as well as possible. Previously, artificial neural networks have been utilized to estimate the nonlinearity in the sensor response of transducers such as pressure sensors and temperature transducers [39]–[41]. However, the sensor presented in this manuscript is significantly more complex and does not involve just one output variable as a function of another operating variable. The sensor presented in this manuscript provides three output variables (normal force, shear force, and force direction). These three output variables are a function of the four capacitances and also have to be calibrated with the stiffness which varies depend on the angular location around the sensor. Due to the large number of variables and data involved, simple calibration curves cannot be utilized, and a deep learning neural network was required.

A two-layer feed-forward network with sigmoid hidden neurons and linear output neurons, is designed to fit this multi-dimensional mapping problems as shown in Fig. 8. The

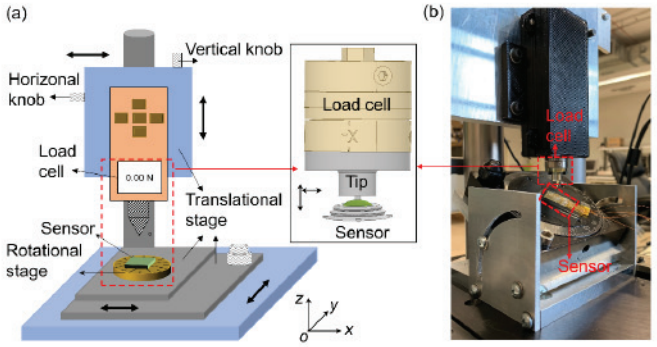

Fig. 9. (a) The schematic and (b) photo of the experimental setup.

capacitance readings of the four sensing units are fed into the neural network as the inputs, while the 3D forces (measured by a load cell during training) are used as the output of the neural network. The network is trained with Levenberg-Marquardt backpropagation algorithm [42]. The resulting trained neural network then serves as the sensor model which can correctly provide the shear and normal components of the force.

III. Experimental Setup

In order to collect sufficient datasets for training the neural network that models the sensor response, the assembled force sensor is tested with a custom-designed experimental setup (Fig. 9), which includes two translational stages (one X-Y stage for coarse tuning and one X-Z stage for fine tuning), a rotational stage and a six-axis load cell (ATI, Nano 17) and a pointed tip attached to the load cell. The pointed tip (~500um in diameter) is chosen to make sure the force is applied at the center of the sensor. At the center of the hard cap of the sensor there is small hole matching the size of the tip. During test, the tip was adjusted through the translational stages and positioned inside the hole. The sensor is fixed on the rotational stage, which is installed on the coarse X-Y translational stage on the bottom. The load cell is fixed on the fine X-Z translational stage over the sensor. By moving the X-Y translational stage down by rotating the vertical knob, varying normal force can be applied on the supercapacitive sensor from the top through a load cell and the tip. By rotating the horizontal knob on the fine stage, shear force along X-axis can be applied. By changing the angle (θ) of the rotational stage, shear forces from all the orientation on the local sensor coordinate can be applied. The reference force readings can be recorded by the load cell simultaneously. The response of each sensor is recorded (Rigol DM3068) with the changing force. So, the vertical displacement z, the horizontal displacement x of fine translational stage on the top, and the rotational angle of rotational stage (also the rotational angle of the sensor) θ are the three varying parameters during the test. Using this setup, all combinations of different shear and normal forces applied on the sensor can be created by changing the combinations of the 3 parameters $[x_i, y_i, \theta_i]$. The forces are applied in steps of small force changes in each axis.

To collect enough datasets for training, the following experimental procedure is used:

TABLE III
NORMAN AND SHEAR FORCES COLLECTED AT $\theta = 45°$

$\theta = 45°$						
	$Fz\ (N)$					
	0.4	0.6	0.7	0.8	0.9	1.0N
Fs (N)	0.05	0.1	0.1	0.1	0.1	0.1
	0.1	0.2	0.2	0.2	0.2	0.2
	…	…	…	…	…	…
	1	1	1	1	1	1

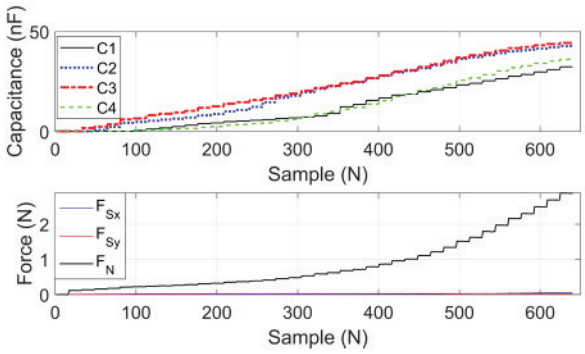

Fig. 10. Sensor response mainly under gradually changing normal force.

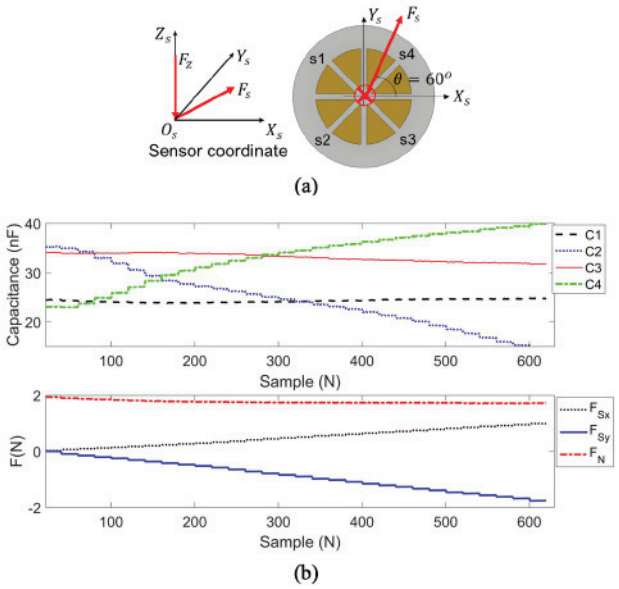

Fig. 11. (a) Normal and shear force in the sensor coordinate at $\theta = 60^{\circ}$. (b) Sensor response under gradually changing shear force ($\theta = 60^{\circ}$) and a constant normal force.

1. First the pointed tip is aligned with the center of the sensor by moving the coarse X-Y translational stage on the bottom;
2. The fine translational stage is moved down to add a normal force F_z on the sensor, then the z displacement is kept steady;
3. The horizontal knob is turned to apply a shear force $F_s(F_x, F_y)$ gradually, then the sensor readings and load cell measurements are recorded.
4. The rotational stage is rotated by 15°, steps (1)-(3) are repeated until $\theta = 360°$.

For example, at $\theta = 45°$, 6 different normal forces are applied, while under each normal force, a series of shear forces are applied as shown in Table III.

Additionally, in order to investigate the influence of parasitic noise on the force sensor, a water-proofed embodiment of the supercapacitive sensor was dipped inside water. The capacitance response of the sensor is recorded while it is outside water and inside water. The increased capacitance after being put inside water is regarded as the parasitic capacitance and is measured.

IV. RESULTS AND DISCUSSION

A. Normal Force Test

The response of the sensor under gradually changing normal force is shown in Fig. 10. The sensitivity of the sensors to normal force along z-axis can reach as high as $50nF/N$, which is more than 1000 times higher than the sensitivity of conventional capacitive sensors [43], [44]. As seen in the figure, all 4 capacitances rise monotonically with increase in the normal force. The maximum normal force applied on the sensor during this test is around 3N, which is adequate for almost all typical skilled hand operations.

B. Normal and Shear Force Test

Normal force and shear force are tested together, since in many cases in real-life, shear force is applied along with normal force. Fig. 11 shows an example of the sensor response when both normal and shear forces are applied, with normal force being held as roughly constant to study the capacitance response with changing shear forces. The applied normal force is around $1.7N$. The shear force applied is at θ =60°, which is towards S_4, in the local sensor coordinate as shown in Fig.11 (a). As shown in Fig.11 (b), C_4 capacitance increases, while the readings from C_2 changes to an opposite direction. C_1 experiences a minor increase in capacitance reading, while the C_3 decreases a little. The sensitivity of the sensor to shear force can reach as high as $22nF/N$, which is smaller than that to the normal force due to the higher stiffness along the horizontal direction of the sensor. The maximum shear force applied on the sensor during this test is around 1.6N.

A curve fitting method was used first based on the linear model in Equations (2-4). Data was collected at a random angle following the test procedure. Three tests were conducted at 3 different fixed normal forces. As shown in Fig. 12, the sensor response is non-linear and calibration coefficients K_{s1}, K_{s2}, K_{s3} and K_{s4} that work well when $F_{s3} = 1.1N$ (Fig.12 (c)) cannot provide accurate force estimation when $F_{s3} = 0.75N$. Hence, a model that accounts for the varying stiffness with varying θ is required.

A learning method was therefore utilized to train a better model. By following the test procedure described above, 32,000 datasets including sensor responses (C_1, C_2, C_3, C_4), and load cell measurements (F_x, F_y, F_z) are collected and

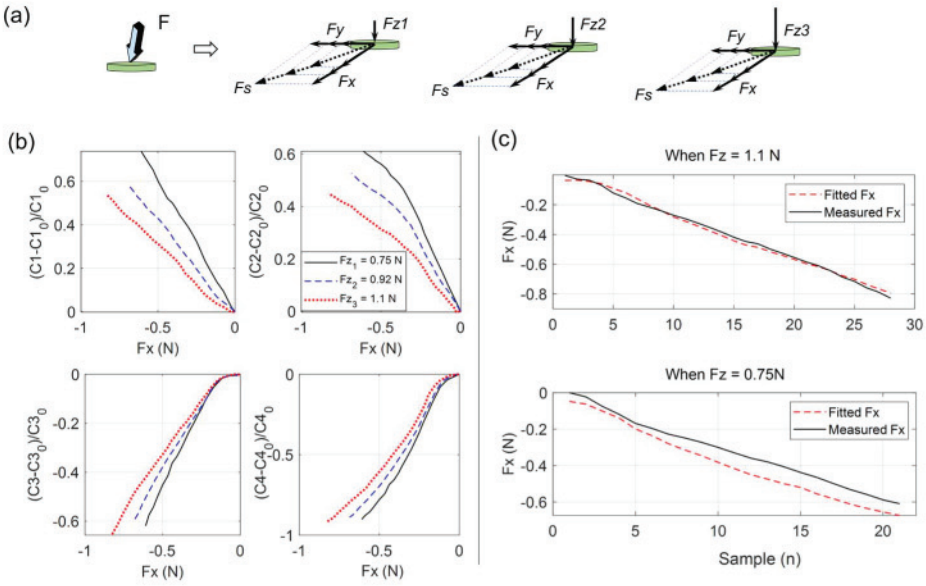

Fig. 12. An example of curving fitting based on the linear equations. (a) constant normal forces with gradually increased shear forces (3 tests with 3 constant normal forces) (b) normalized capacitance changes with increase Fx, (c) curve fitting results.

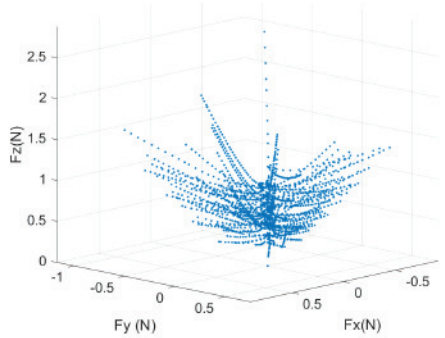

Fig. 13. Force datasets in a 3D plot.

used to train a model for the sensor using deep learning. All the datasets used for training are shown in the 3D plot in Fig. 13. 350 datasets are left aside, not used for training and used separately to validate the performance of the model.

An example validation using a dataset not used in training the neural network model is shown in Fig. 14. The applied normal force is around $1.0N$. The shear force applied is at $\theta \approx 265°$, which is towards S_2 and S_3, in the local sensor coordinate as shown in Fig. 14(a). The sensor response as shown in Fig. 14(b) is fed into the previously trained model. As shown in Fig. 14(c), the fitted forces using the trained model and the real measured forces match well, with a maximum error of $0.02N$. The dynamic range of the sensor shear force can reach as high as 80:1. (The dynamic range is defined in this work as force range divided by force resolution.) It should be noted that this value could be larger since the maximum range of the sensor is not reached in this work.

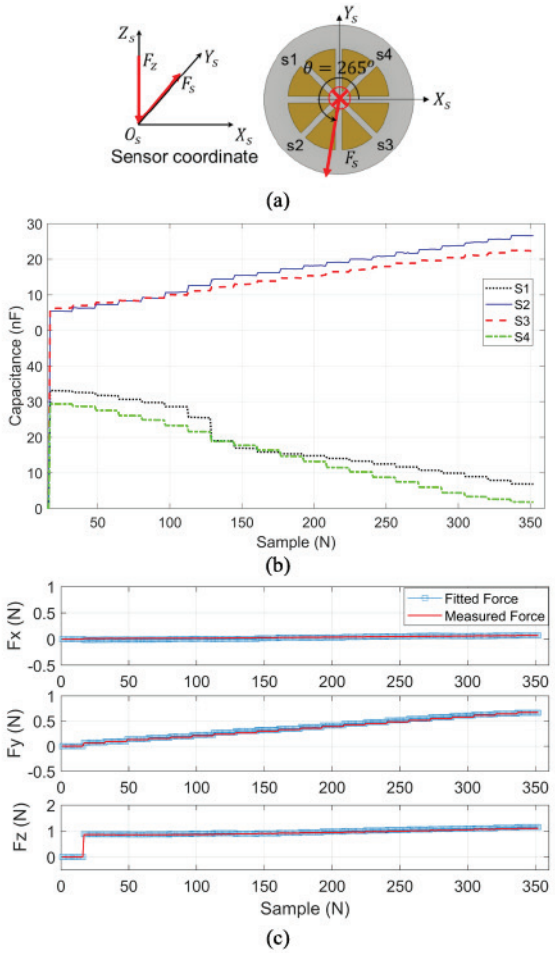

Fig. 14. (a) Normal and shear force in the sensor coordinate at $\theta = 265°$ for validation, (b) capacitance measurement at $\theta = 265°$ for validation (c) estimated forces using the neural network fitted model.

C. Inside Water Test

In the case of a traditional parallel plate capacitor, fringe electrical field outside the plates of the capacitor penetrates neighboring materials as shown in Fig. 15 (a) and builds additional capacitance, which is called parasitic capacitance. For in vivo applications, where the capacitive sensor is in

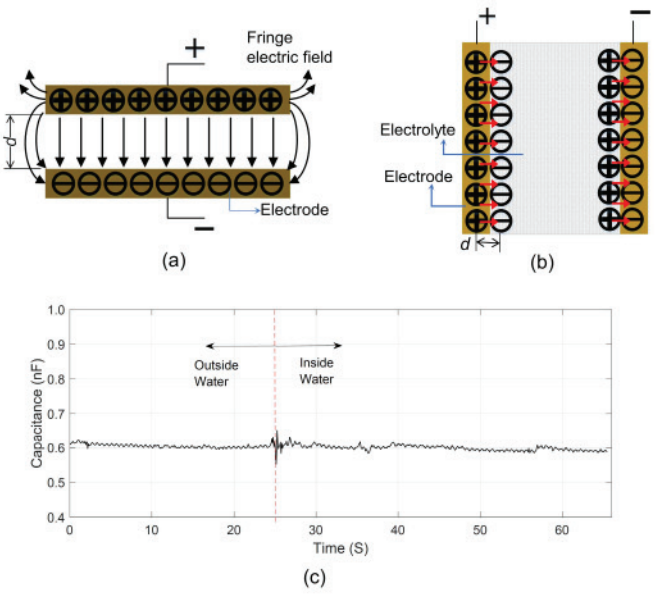

Fig. 15. (a) Fringe electric field on a capacitive sensor, (b) schematic of a supercapacitive sensor. (c) Normal and shear force in the sensor coordinate at $\theta = 60^{\circ}$.

a liquid environment, due to the large dielectric constant of water and tissues that surround the sensor, the magnitude of the parasitic capacitance can be relatively large (10s of pico Farads, pF) [45], compared to the small direct response of a traditional capacitive sensor.

Measures could be taken to the remove this parasitic noise. Parasitic capacitance can be compensated by measurement in the absence of loads and subsequent subtraction, but this is only possible when the parasitic noise is static. In biomedical in vivo applications of the capacitive sensors, the interference from human tissues on the fringe electric field of the sensor can cause dynamic parasitic noise, which can greatly pollute the sensor signal and cannot be eliminated by subtraction. Another method has been explored to remove the parasitics by using an active Faraday cage [45]. However, there was still significant parasitic capacitance left and this method involves a complex fabrication process in order to create a highly conductive Faraday cage that surrounds the entire sensor. In a supercapacitive sensor, the distance between the positive and negative charges at each electrode is of the order of the size of one or two atomic layers (Fig. 15 (b)). Hence, the fringe fields which results in parasitic noise in liquid environment are negligible compared to that on a traditional capacitive sensor. Furthermore, the high capacitance in the supercapacitor overwhelms the parasitic capacitance. Therefore, we hypothesize that when being used in liquid environments like in vivo use, the normal-shear sensor based on supercapacitive sensing will not experience additional parasitic noise.

The result for the in-water test is shown in Fig. 15 (c). After dipping into the water, the capacitance increases by a small amount ranging from $1pF10pF$, starting from a base capacitance of $600pF$, which includes variations from instrument errors and also the sensor response caused by the water pressure. This increase in capacitance in the presence of water is negligible compared to the ultra-high sensitivity of the sensor at $\sim 22nF/N$. That indicates that the sensor is immune from parasitic noise and can be used in wet environments, such as inside the human body. This is also very important for applications of the shear and normal force sensor on domestic robots since liquid environments can be encountered by a robot during domestic chores.

V. Conclusion

This paper developed a thin normal-shear force sensor based on the use of a supercapacitive sensing mechanism. The sensor had a quad structure with four sensing units in which the bottom substrate has four pairs of electrodes while the top deformable portion has a solid-state electrolyte. The sensing mechanism was based on the increase in contact area between the solid-state electrolyte and the electrodes upon application of normal and/or shear forces. Key innovations in the sensing mechanism included the use of a paper-based solid state electrolyte, the use of 3d-printing with a combination of soft and hard polymers to construct the top portion of the sensor, and the use of deep learning to model the sensor response. The sensor can accept any combination of shear and normal forces and can measure both their magnitudes and orientation.

The sensor was designed and fabricated using MEMS technologies and 3D printing. A model of the sensor was constructed using a neural network and an associated learning algorithm with reference training data. This enabled the sensor system to provide accurate normal and shear force measurements irrespective of the direction in which the force is applied and irrespective of the stiffness variations along the circumference of the sensor.

The influence of parasitic noise was investigated by dipping the sensor inside water. The experimental results showed preliminary data to indicate that the sensor has high sensitivity, high dynamic range and negligible parasitic capacitance.

The developed shear and normal force sensor is unique, exploiting the high sensitivity and range of the supercapacitive sensor. A number of experiments were carried out to evaluate the performance of the shear and normal force sensor using a custom-designed setup with a load cell, translational stands, and rotational stand. The influence of parasitic noise was investigated by dipping the sensor inside water and measuring its resulting capacitance change. The performance of the sensor was presented in the Results and Discussion section. The sensitivity of the sensor to normal force can reach as high as $50nF/N$ and that to shear force is $22nF/N$, that is more than 1000 times than that of traditional capacitive sensors. The developed sensor is tested under loads up to 3N, which is more than typical forces on the fingertips while handling many household tasks. Besides, experimental test results have shown that the sensor is immune from parasitic noise. This is also very important for applications of the glove with shear and normal force sensor on domestic robots since liquid environments can be encountered by the robot during domestic chores. All of these results together indicate that the develop shear and normal force sensor can be used on an instrumented glove as a viable device for actual use.

The integrated sensor was developed to measure both and normal forces simultaneously. It uses an omni-directional structure capable of multi-axis sensing while using a rapid and simple fabrication process to reduce time and costs associated with previous shear and normal force sensors. High resolution 3D printing with materials of different mechanical properties provides flexible fabrication process. While other researchers have previously explored shear and normal force sensors from a fundamental research perspective [18], [24], [27], this is the first time that such a shear and normal force sensor proposes a way to estimate forces quantitatively using a model obtained by neuro network and matching the experimental data as well as possible. Forces applied from random directions can be obtained using the model, instead of just the forces on the two major axes.

The success of the preliminary experiments conducted in this paper opens up the possibility that future work could be conducted that involves integrating multiple such sensors on an instrumented glove and measuring forces on the fingertips in various applications and evaluating the forces on the hands during various human activities. Such a glove could find applications in medical and health care, sports, laboratory research, and robotics.

REFERENCES

[1] Tekscan. *Pressure Mapping, Force Measurement & Tactile Sensors*. Accessed: Mar. 28, 2020. [Online]. Available: https://www.tekscan.com/pressure-sensors?utm_source=google&utm_medium=cpc&utm_term=sitelink&utm_content=pressure+sensors&utm_campaign=corporate&utm_source=google&utm_medium=cpc&utm_term=tekscan&utm_content=eta1&utm_campaign=corporate&gclid=Cj0KCQiAtOjyBRC

[2] L. Dipietro, A. M. Sabatini, and P. Dario, "A survey of glove-based systems and their applications," *IEEE Trans. Syst., Man, Cybern. C, Appl. Rev.*, vol. 38, no. 4, pp. 461–482, Jul. 2008.

[3] R. C. King, L. Atallah, B. Lo, and G.-Z. Yang, "Development of a wireless sensor glove for surgical skills assessment," *IEEE Trans. Inf. Technol. Biomed.*, vol. 13, no. 5, pp. 673–679, Sep. 2009.

[4] Q. Ye, M. Seyedi, Z. Cai, and D. T. H. Lai, "Force-sensing glove system for measurement of hand forces during motorbike riding," *Int. J. Distrib. Sensor Netw.*, vol. 11, no. 11, Nov. 2015, Art. no. 545643.

[5] M. K. Kim *et al.*, "Soft-packaged sensory glove system for human-like natural interaction and control of prosthetic hands," *NPG Asia Mater.*, vol. 11, no. 1, pp. 1–12, Dec. 2019.

[6] G. Singh, S. Boddu, I. Chakravorty, G. M. Bairy, and M. Ganesh, "An instrumented glove for monitoring forces during object manipulation," in *Proc. IEEE Point-Care Healthcare Technol. (PHT)*, Jan. 2013, pp. 212–215.

[7] Y. Park, J. Lee, and J. Bae, "Development of a wearable sensing glove for measuring the motion of fingers using linear potentiometers and flexible wires," *IEEE Trans. Ind. Informat.*, vol. 11, no. 1, pp. 198–206, Feb. 2015.

[8] J.-H. Kim, N. D. Thang, and T.-S. Kim, "3-D hand motion tracking and gesture recognition using a data glove," in *Proc. IEEE Int. Symp. Ind. Electron.*, Jul. 2009, pp. 1013–1018.

[9] L. Wang and D. J. Beebe, "A silicon-based shear force sensor: Development and characterization," *Sens. Actuators A, Phys.*, vol. 84, nos. 1–2, pp. 33–44, Aug. 2000.

[10] R. D. Ponce, J. D. Posner, and V. J. Santos, "Flexible microfluidic normal force sensor skin for tactile feedback," *Sens. Actuators A, Phys.*, vol. 179, pp. 62–69, Jun. 2012.

[11] L. Wang and D. J. Beebe, "Characterization of a silicon-based shear-force sensor on human subjects," *IEEE Trans. Biomed. Eng.*, vol. 49, no. 11, pp. 1340–1347, Nov. 2002.

[12] L. Beccai *et al.*, "Design and fabrication of a hybrid silicon three-axial force sensor for biomechanical applications," *Sens. Actuators A, Phys.*, vol. 120, no. 2, pp. 370–382, May 2005.

[13] E.-S. Hwang, J.-H. Seo, and Y.-J. Kim, "A polymer-based flexible tactile sensor for both normal and shear load detections and its application for robotics," *J. Microelectromech. Syst.*, vol. 16, no. 3, pp. 556–563, Jun. 2007.

[14] X. Shi, C.-H. Cheng, Y. Zheng, and P. K. A. Wai, "An EGaIn-based flexible piezoresistive shear and normal force sensor with hysteresis analysis in normal force direction," *J. Micromech. Microeng.*, vol. 26, no. 10, Oct. 2016, Art. no. 105020.

[15] T. Iwasaki *et al.*, "Shearing force measurement device with a built-in integrated micro displacement sensor," *Sens. Actuators A, Phys.*, vol. 221, pp. 1–8, Jan. 2015.

[16] T. Takeshita, K. Harisaki, H. Ando, E. Higurashi, H. Nogami, and R. Sawada, "Development and evaluation of a two-axial shearing force sensor consisting of an optical sensor chip and elastic gum frame," *Precis. Eng.*, vol. 45, pp. 136–142, Jul. 2016.

[17] M.-Y. Cheng, C.-L. Lin, Y.-T. Lai, and Y.-J. Yang, "A polymer-based capacitive sensing array for normal and shear force measurement," *Sensors*, vol. 10, no. 11, pp. 10211–10225, Nov. 2010.

[18] L. Viry *et al.*, "Flexible three-axial force sensor for soft and highly sensitive artificial touch," *Adv. Mater.*, vol. 26, no. 17, pp. 2659–2664, May 2014.

[19] T. Nakadegawa, H. Ishizuka, and N. Miki, "Three-axis scanning force sensor with liquid metal electrodes," *Sens. Actuators A, Phys.*, vol. 264, pp. 260–267, Sep. 2017.

[20] F. Zhu and J. W. Spronck, "A capacitive tactile sensor for shear and normal force measurements," *Sens. Actuators A, Phys.*, vol. 31, nos. 1–3, pp. 115–120, Mar. 1992.

[21] S. Somlor, A. Schmitz, R. S. Hartanto, and S. Sugano, "First results of tilted capacitive sensors to detect shear force," *Procedia Comput. Sci.*, vol. 76, pp. 101–106, Dec. 2015.

[22] T. A. Chase and R. C. Luo, "A thin-film flexible capacitive tactile normal/shear force array sensor," in *Proc. 21st Annu. Conf. IEEE Ind. Electron. (IECON)*, Nov. 1995, pp. 1196–1201.

[23] R. D. P. Wong, J. D. Posner, and V. J. Santos, "Flexible microfluidic normal force sensor skin for tactile feedback," *Sens. Actuators A, Phys.*, vol. 179, pp. 62–69, Jun. 2012.

[24] H.-K. Lee, J. Chung, S.-I. Chang, and E. Yoon, "Normal and shear force measurement using a flexible polymer tactile sensor with embedded multiple capacitors," *J. Microelectromech. Syst.*, vol. 17, no. 4, pp. 934–942, Aug. 2008.

[25] H.-K. Lee, J. Chung, S.-I. Chang, and E. Yoon, "Polymer tactile sensing array with a unit cell of multiple capacitors for three-axis contact force image construction," in *Proc. IEEE 20th Int. Conf. Micro Electro Mech. Syst. (MEMS)*, Jan. 2007, pp. 623–626.

[26] J. A. Dobrzynska and M. A. M. Gijs, "Polymer-based flexible capacitive sensor for three-axial force measurements," *J. Micromech. Microeng.*, vol. 23, no. 1, Jan. 2013, Art. no. 015009.

[27] H.-K. Lee, J. Chung, S.-I. Chang, and E. Yoon, "Real-time measurement of the three-axis contact force distribution using a flexible capacitive polymer tactile sensor," *J. Micromech. Microeng.*, vol. 21, no. 3, Mar. 2011, Art. no. 035010.

[28] P. Roberts, D. D. Damian, W. Shan, T. Lu, and C. Majidi, "Soft-matter capacitive sensor for measuring shear and pressure deformation," in *Proc. IEEE Int. Conf. Robot. Autom.*, May 2013, pp. 3529–3534.

[29] Y. Zhang, R. Rajamani, and S. Sezen, "Novel supercapacitor-based force sensor insensitive to parasitic noise," *IEEE Sensors Lett.*, vol. 1, no. 6, Dec. 2017 Art. no. 1500704.

[30] A. Charalambides and S. Bergbreiter, "A novel all-elastomer MEMS tactile sensor for high dynamic range shear and normal force sensing," *J. Micromech. Microeng.*, vol. 25, no. 9, Sep. 2015, Art. no. 095009.

[31] Y. Zhang and L. Li, "Modelling and design of MEMS piezoresistive out-of-plane shear and normal stress sensors," *Sensors*, vol. 18, no. 11, p. 3737, Nov. 2018.

[32] M. N. M. Nawi, A. A. Manaf, M. F. A. Rahman, M. R. Arshad, and O. Sidek, "One-side-electrode-type fluidic-based capacitive pressure sensor," *IEEE Sensors J.*, vol. 15, no. 3, pp. 1738–1746, Mar. 2015.

[33] B. Nie, S. Xing, J. D. Brandt, and T. Pan, "Droplet-based interfacial capacitive sensing," *Lab Chip*, vol. 12, no. 6, pp. 1110–1118, Jul. 2012.

[34] Y. Zhang, S. Sezen, M. Ahmadi, X. Cheng, and R. Rajamani, "Paper-based supercapacitive mechanical sensors," *Sci. Rep.*, vol. 8, no. 1, p. 16284, 2018.

[35] M. Taufik and P. Jain, "Role of build orientation in layered manufacturing: A review," *Int. J. Manuf. Technol. Manag.*, vol. 27, nos. 1–3, pp. 47–73, Jan. 2014.

[36] P. Diagrams and M. Word, "Neural network ensembles, cross validation, and active learning anders," in *Proc. Adv. Neural Netw. Process. Syst.*, vol. 7, 2010, pp. 6–7.

[37] D. F. Specht, "A general regression neural network," *IEEE Trans. Neural Netw.*, vol. 2, no. 6, pp. 568–576, Nov. 1991.
[38] S. Haykin, *Neural Networks: A Comprehensive Foundation*, 2nd ed. Upper Saddle River, NJ, USA: Prentice-Hall PTR, 1998.
[39] J. C. Patra, G. Panda, and R. Baliarsingh, "Artificial neural network-based nonlinearity estimation of pressure sensors," *IEEE Trans. Instrum. Meas.*, vol. 43, no. 6, pp. 874–881, Dec. 1994.
[40] J. C. Patra, A. C. Kot, and G. Panda, "An intelligent pressure sensor using neural networks," *IEEE Trans. Instrum. Meas.*, vol. 49, no. 4, pp. 829–834, Aug. 2000.
[41] K. V. L. Narayana and V. N. Kumar, "Development of an intelligent temperature transducer," *IEEE Sensors J.*, vol. 16, no. 12, pp. 4696–4703, Jun. 2016.
[42] A. Reynaldi, S. Lukas, and H. Margaretha, "Backpropagation and Levenberg-Marquardt algorithm for training finite element neural network," in *Proc. 6th UKSim/AMSS Eur. Symp. Comput. Modeling Simulation*, no. 2, Nov. 2012, pp. 89–94.
[43] M. Ahmadi, R. Rajamani, and S. Sezen, "Transparent flexible active Faraday cage enables *in vivo* capacitance measurement in assembled microsensor," *IEEE Sensors Lett.*, vol. 1, no. 5, Oct. 2017, Art. no. 2500604.
[44] M. Ahmadi, R. Rajamani, G. Timm, and A. S. Sezen, "Flexible distributed pressure sensing strip for a urethral catheter," *J. Microelectromech. Syst.*, vol. 24, no. 6, pp. 1840–1847, Dec. 2015.
[45] M. Ahmadi, R. Rajamani, and S. Sezen, "Transparent flexible active Faraday cage enables *in vivo* capacitance measurement in assembled microsensor," *IEEE Sensors Lett.*, vol. 1, no. 5, pp. 1–4, Oct. 2017.

Ye Zhang received the bachelor's and master's degrees in vehicle engineering from Tongji University, Shanghai, China, in 2011 and 2013, respectively, and the Ph.D. degree from the Department of Mechanical Engineering, The University of Minnesota at Twin Cities, Minneapolis, MN, USA.

While completing her studies in the fields of sensing and medical devices, she worked with the university as a member of the Laboratory for Innovations in Sensing, Estimation, and Control. Her pending patent in doctoral research focused on developing a novel type of paper-based supercapacitive sensor and customizing it for a variety of biomedical applications.

A. Serdar Sezen received the B.S. and M.S. degrees in mechanical engineering from Middle East Technical University, Ankara, Turkey, in 1999 and 2001, respectively, and the Ph.D. degree in mechanical engineering from The University of Minnesota at Twin Cities, Minneapolis, MN, USA, in 2006.

He is currently a Professor of Mechanical Engineering with the Department of Mechanical and Manufacturing Engineering, St. Cloud State University, St. Cloud, MN, USA, where he has been a Faculty Member since 2008. He has coauthored over 20 journal articles, holds three patents, has supervised over 20 industry-sponsored projects, and consulted with several companies in his research areas. His research and professional interest focuses on sensor development, especially in the areas of biomedical systems, dynamic systems, mechanical design, product design, industrial controls, industrial automation, and robotics.

Rajesh Rajamani (Senior Member, IEEE) received the B.Tech. degree from the Indian Institute of Technology at Madras in 1989, and the M.S. and Ph.D. degrees from the University of California at Berkeley in 1991 and 1993, respectively.

He is currently the Benjamin Y. H. Liu-TSI Endowed Professor of Mechanical Engineering with The University of Minnesota at Twin Cities. His active research interests include sensing, estimation, and control for smart mechanical systems. Several inventions from his laboratory have been commercialized through start-up ventures co-founded by industry executives. One of these companies, Innotronics, was recently recognized among the 35 Best University Start-Ups of 2016 in a competition conducted by the U.S. National Council of Entrepreneurial Tech Transfer. He has coauthored over 150 journal articles and is a co-inventor of 16 patent applications. He has authored a popular book *Vehicle Dynamics and Control* (Springer–Verlag). He is a Fellow of the ASME and has been a recipient of the CAREER Award from the National Science Foundation, the Ralph Teetor Award from the SAE, the O. Hugo Schuck Award from the American Automatic Control Council, and a number of best paper awards from journals and conferences. He has served as the Chair of the IEEE Technical Committee on Automotive Control and on the Editorial Boards of the IEEE TRANSACTIONS ON CONTROL SYSTEMS TECHNOLOGY, the IEEE/ASME TRANSACTIONS ON MECHATRONICS, and the *IEEE Control Systems Magazine*.